



Applicability of InSAR Monitoring of the Reykjanes Peninsula

Deformation and Strain

Vincent Drouin

Prepared for Landsnet

ÍSOR-2021/004

ICELAND GEOSURVEY

Reykjavík: Orkugardur, Grensásvegur 9, 108 Reykjavík, Iceland - Tel.: 528 1500 - Fax: 528 1699

Akureyri: Rangárvellir, P.O. Box 30, 602 Akureyri, Iceland - Tel.: 528 1500 - Fax: 528 1599

isor@isor.is - www.isor.is

Applicability of InSAR Monitoring of the Reykjanes Peninsula

Deformation and Strain

Vincent Drouin

Prepared for Landsnet

ÍSOR-2021/004

March 2021

Report no. ÍSOR-2021/004	Date March 2021	Distribution <input checked="" type="checkbox"/> Open <input type="checkbox"/> Closed
Report name / Main and subheadings Applicability of InSAR Monitoring of the Reykjanes Peninsula. Deformation and Strain.		Number of copies 1
		Number of pages 15
Authors Vincent Drouin		Project manager Ásdís Benediktsdóttir
Classification of report		Project no. 21-0004
Prepared for Landsnet		
Cooperators		
Abstract Interferometric Synthetic Aperture Radar (InSAR) is a remote sensing technique allowing to measure deformation with mm-precision over large areas. It has been used since the early 90's to monitor natural hazard and anthropogenic deformation. This report presents a short description of the technique, as well as two examples of the application of the technique regarding deformation over the Reykjanes Peninsula. The first example gives an overview of long-term tectonic and anthropogenic deformation between 2015 and 2018 for the entire peninsula. The second example is focused on the co-seismic displacements associated with an M5.6 earthquake happening on the 20 th of October 2020 in the center of the peninsula.		
Key words InSAR, Reykjanes, earthquake, strain rate, Landsnet, ÍSOR		Project manager's signature <i>Ásdís Benediktsdóttir</i>
		Reviewed by Egill Árni Guðnason, Arnar Már Vilhjálmsson

Table of contents

1	Introduction to InSAR	7
1.1	SAR.....	7
1.2	InSAR.....	7
2	Deformation in Reykjanes	8
2.1	2015–2018 velocities	8
2.2	Earthquake deformation: 20 th October 2020 example	10
2.3	Volcanic unrest: early 2021 example	10
3	Conclusions	14
4	References	15

List of figures

Figure 1.	<i>Near-East and near-Up average velocities between summer 2015 and summer 2018</i>	9
Figure 2.	<i>Near-East and near-Up total co-seismic displacements for the 20th Oct. 2020 earthquake</i> . 12	12
Figure 3.	<i>Near-East and near-Up total displacements between the 23rd February and the 8th March 2021</i>	13
Figure 4.	<i>Focal mechanism of a selection of large earthquakes (magnitude > 4.8) that occurred on the 24th of February and onwards, shown in the location of the earthquake</i>	14

1 Introduction to InSAR

1.1 SAR

Synthetic Aperture Radar (SAR) is one type of radar imaging. A radar instrument sends a pulse of energy and measures how much of it is reflected. The resolution of a traditional radar sensor is directly correlated with the size of its antenna, i.e. the longer the antenna the better the resolution. A radar instrument in space at an altitude of 800 km and with a 10 m long antenna has a pulse resolution of about 5 km, which is unexploitable. However, the same point on the ground will be seen by many pulses. Therefore, the motion of the satellite can be used to generate a synthetic km-long antenna. This allows to achieve a resolution of a few meters, even sub-meter for specific acquisition modes.

The two main information recorded by a SAR instrument are the amplitude of the signal (how much energy is reflected by the ground) and its phases (a value between $-\pi$ and π).

1.2 InSAR

The principle of interferometric SAR (InSAR) is to compare the phase between two SAR acquisitions. The two acquisitions need to be acquired from the exact same location, otherwise no signal can be extracted. The basic processing is to align very precisely the two acquisitions by using their amplitude signal. Once this is done, the phase from both acquisitions can be subtracted to form an interferogram.

$$\varphi_{interferogram} = \varphi_{acquisition_1} - \varphi_{acquisition_2}$$

The phases of this interferogram contain various signals: deformation, satellite orbits, topography, atmosphere, and noise.

$$\varphi_{interferogram} = \varphi_{deformation} + \varphi_{orbits} + \varphi_{topography} + \varphi_{atmosphere} + \varphi_{noise}$$

For deformation studies we try to isolate the deformation part of the signal. To do so, we correct for the satellite orbits using known orbital parameters and for the topography using a high-resolution digital elevation model (DEM). The atmosphere can be corrected for by using weather models for single interferograms and time-series analysis for series of interferograms. The noise can be reduced by spatial filtering.

Once all the corrections have been applied, we obtain a deformation interferogram in the line-of-sight (LOS) of the satellite. This means that we measure the ground deformation along one dimension, away or toward the satellite, unlike GPS, where the deformation is measured in three dimensions. In order to get a better understanding of the deformation, and to have an easier interpretation, it is possible to extract the vertical deformation and the east-west deformation. The principle is to decompose the signal from interferograms covering the same time period but acquired from different point of view. The resulting deformation are called near-East and near-Up to reflect the approximation during the decomposition process.

InSAR has successfully been used to measure a wide range of ground deformation: earthquakes (Massonnet et al., 1993; Pagli et al., 2003), volcanoes (Sigmundsson et al., 2010), landslides (Schlögel et al., 2015), plate tectonics (Vadon & Sigmundsson, 1997; Drouin & Sigmundsson, 2019), geothermal areas (Drouin et al., 2017; Juncu et al., 2017), dams (Wang et al., 2011), etc. InSAR time-series can achieve mm precision of deformation measurements (Ferretti et al., 2007). If the ground surface changes too much between the two acquisitions, then no signal is

recorded. This is usually caused by vegetation growth or snow cover. The former is not an issue in most part of Iceland, but the latter means that deformation measurements can usually not be made during the winter months in snow covered areas.

2 Deformation in Reykjanes

2.1 2015–2018 velocities

The Sentinel-1 SAR mission from the Copernicus program (European Space Agency) is one of the main providers of SAR data. Images are acquired every 6 or 12 days over most of the world and are available free of charge. For Iceland, images were acquired every 12 days between 2015 and 2017 and are acquired every 6-days since 2017. This unprecedented amount of data allowed to create deformation velocity maps for all of Iceland (Drouin & Sigmundsson, 2019). The velocities obtained from InSAR are in a very good agreement with the velocities measured at continuous GPS sites through the country. Figure 1 shows the part of these maps covering the Reykjanes Peninsula for 2015–2018.

We can see that the near-East velocities span about 20 mm/y. This amounts for the plate spreading in Iceland as the Reykjanes Peninsula defines the plate boundary between the North American plate and the Eurasian plate. The near-Up velocities show a subsidence of about -30 mm/y related to geothermal exploitation at the Reykjanes geothermal field (Receveur et al., 2019). Subsidence is also visible at the Svartsengi geothermal field and within the Krýsuvík area.

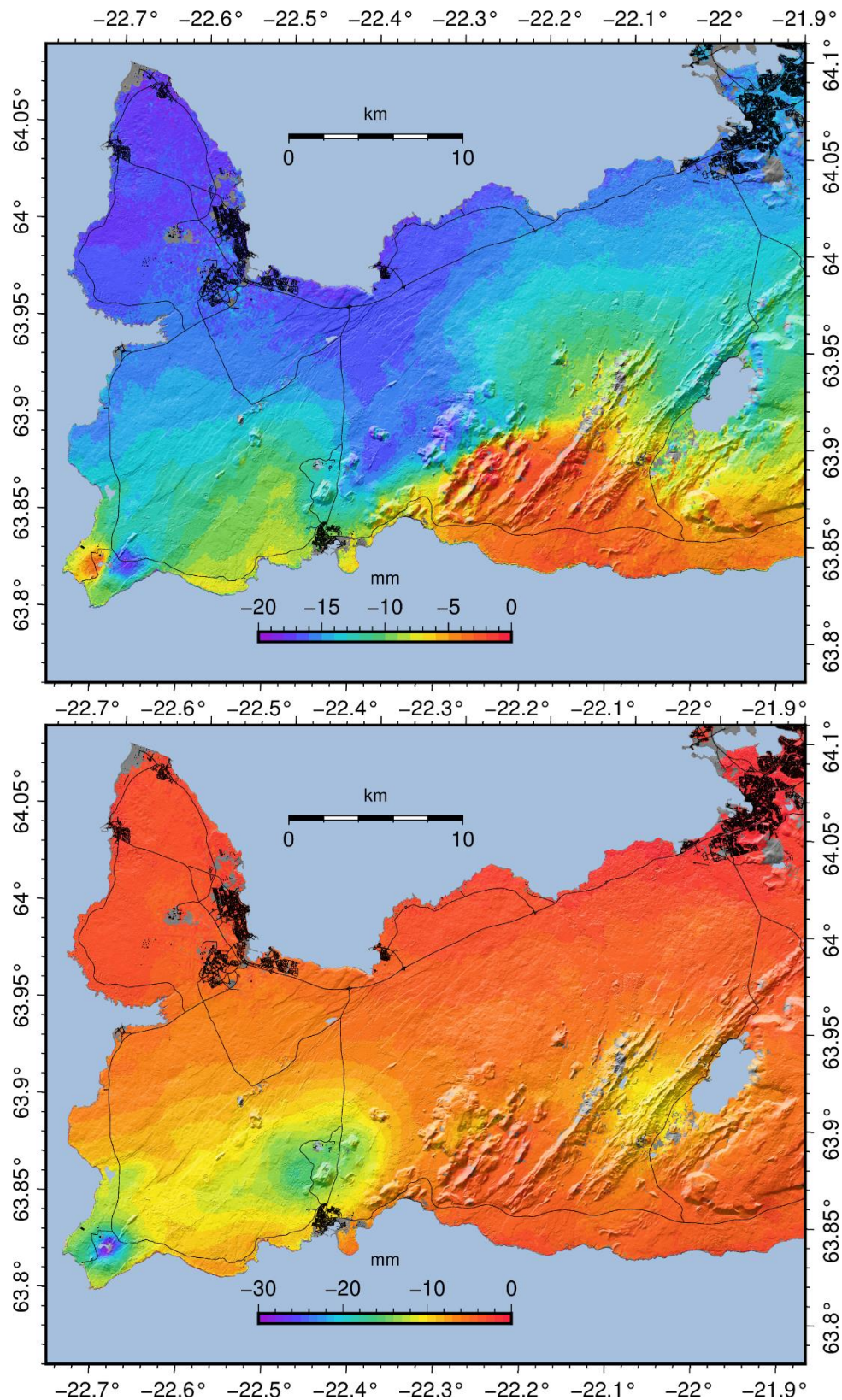


Figure 1. Near-East (top panel) and near-Up (bottom panel) average velocities between summer 2015 and summer 2018 from Drouin & Sigmundsson (2019). Background shows shaded topography, roads (black lines), buildings (black areas), and water (blue/grey areas).

2.2 Earthquake deformation: 20th October 2020 example

On the 20th of October 2020 at approximately 13:43 GMT, an M5.6 earthquake occurred at the center of the Reykjanes Peninsula, about 25 km SW of Reykjavík. It was clearly felt in the capital area and the rest of the peninsula. This was one of the largest earthquakes recorded in the area since the 70's (Björnsson et al., 2020). The Sentinel-1 mission provides two 6-days interferograms covering the event: 20–26 Oct. for the descending track T155 and 16–22 Oct. for the ascending track T16. As described in Section 1.2, the two interferogram signals were decomposed to extract the near-East and near-Up displacements shown in Figure 2. Also, the focal mechanism of the M5.6 earthquake shows right-lateral strike-slip movement on a N-S oriented fault plane, as shown in Figure 2.

We can see that the co-seismic displacements are relatively large, with a total amplitude of around 10 cm for both near-East and near-Up components. By taking the first derivative of the displacement field, we get an image of the strain rate associated with the earthquake. We have highlighted areas of high-strain rate, shown in red color in Figure 2b and 2d. These areas highlight discontinuities in the displacements field and therefore indicate faults which moved during the earthquake. The deformation across these faults is likely to be larger than the values shown on the displacement fields because of the resolution at which the data was analyzed (about 50 m).

2.3 Volcanic unrest: early 2021 example

On the 24th of February 2021 at approximately 10:05 GMT, a M5.7 earthquake occurred near Mt. Fagradalsfjall, Reykjanes Peninsula, about 5 km west of the 20th of October earthquake. Many subsequent earthquakes were observed along the plate boundary from Svartsengi geothermal area to Kleifarvatn Lake. The largest earthquake and most other large earthquakes were right-lateral strike-slip earthquakes happening along N-S faults. In the following days, seismic and InSAR data suggested that a dike was intruding into the crust beneath Mt. Fagradalsfjall and going NE towards Mt. Keilir. On the 3rd of March, another tremor pulse was observed, and the seismicity started to migrate SW from Mt. Fagradalsfjall. The latest interferogram seems to indicate that this activity is caused by a new dike or a prolongation of the previous one, toward the SW. Note that this event is ongoing at the time of the writing and that the current interpretation of the deformation being caused by dikes could change in the future.

The deformation is still on-going in the area and the acquisition are offset by a couple of days between tracks. This means that both ascending and descending interferograms do not cover the same deformation. Therefore, the decomposition process to get the East and Up total displacements is much more uncertain than usual. The results show over 50 cm of East-West deformation and over 30 cm of vertical deformation (Figure 3). Most of this deformation is caused by the diking but earthquakes also have a significant contribution. Dikes travelling within the crust can generate grabens with fault movements in the order of meters (Ruch et al., 2016) but this has not been observed in the current case. Observed fault movements since the beginning of the unrest are most likely associated with earthquakes.

Using the InSAR data shown in Figure 3, visible faults were mapped manually (Figure 4). The InSAR images are noisier than in the case of the 2020 October earthquake which makes it difficult to create a Figure comparable to Figures 2B and 2C. Faults close to the epicenter of the main shock may have moved but no deformation data have been recovered in this area and therefore they could not be mapped.

The line-of-sight (LOS) displacements covering the M5.7 earthquake on the 24th of February show over 10 cm of deformation. This is comparable to the 20th of October earthquake. However much less fractures are visible on the deformation field, indicating that the main fault ruptured mostly at depth unlike in October where the fault propagated to the surface up to 7-8 kilometers to the north.

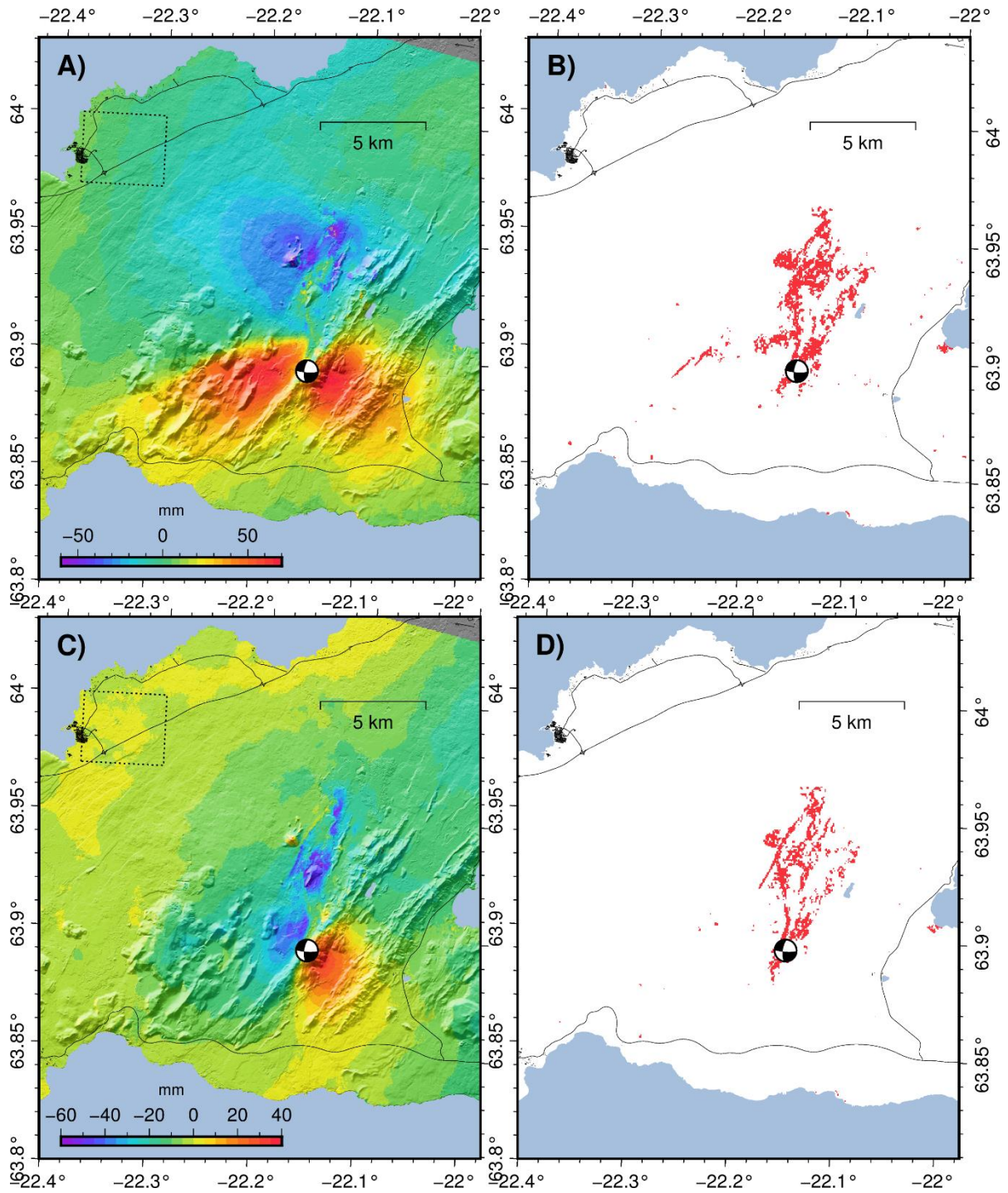


Figure 2. Near-East (A) and near-Up (C) total co-seismic displacements for the 20th October 2020 earthquake. High-strain areas (red) for near-East (B) and near-Up components (D). Background shows the main earthquake focal mechanism (data: Veðurstofa Íslands, Czech Academy of Science, ÍSOR, Orka náttúrunnar; processing: Þorbjörg Ágústsdóttir & Egill Árni Guðnason, ÍSOR), the reference area (dashed area), shaded topography, roads (black lines), buildings (black areas, and water (blue/grey areas).

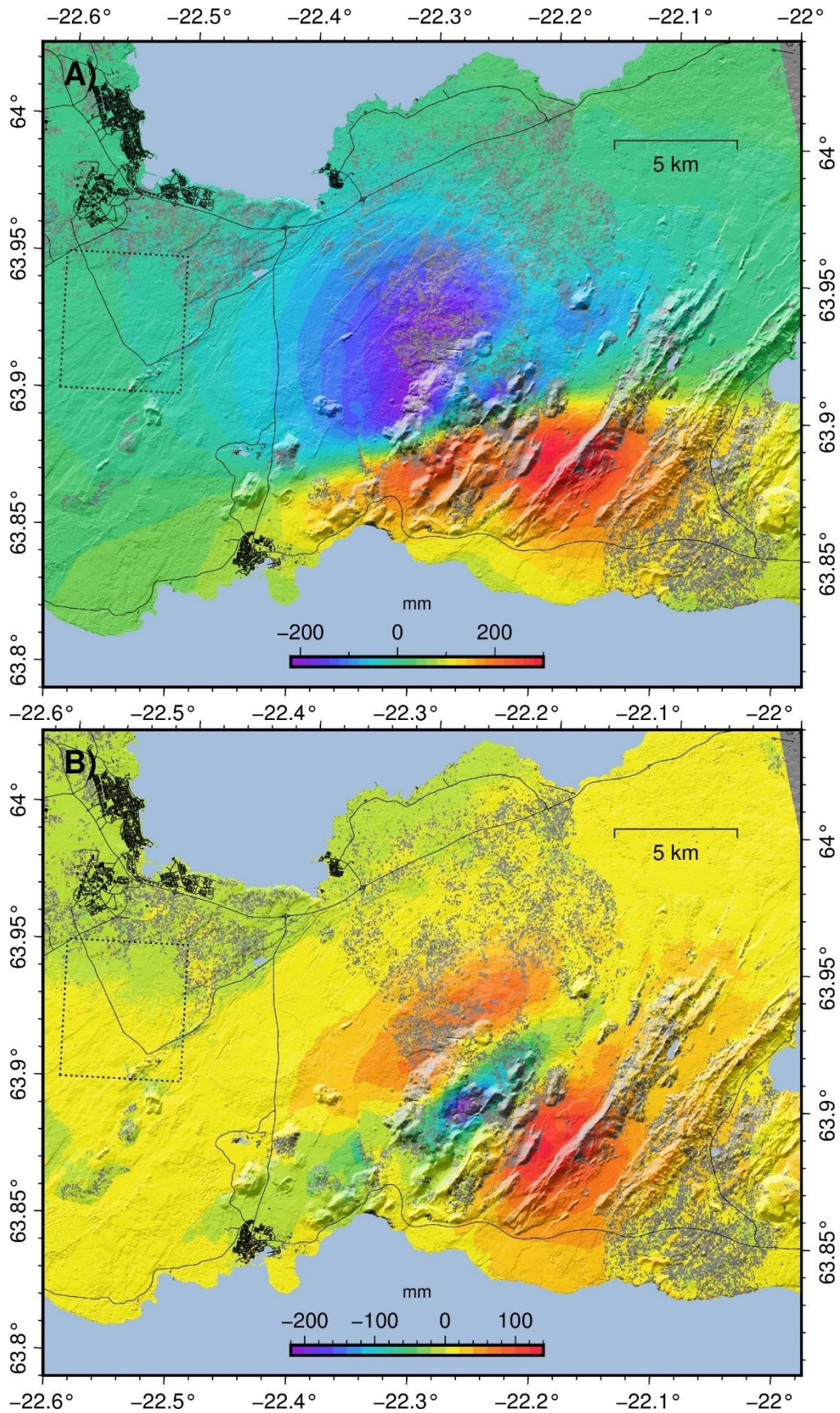


Figure 3. Near-East (A) and near-Up (B) total displacements between the 23rd February and the 8th March 2021. Background shows the reference area (dashed area), shaded topography, roads (black lines), buildings (black areas), and water (blue/grey areas).

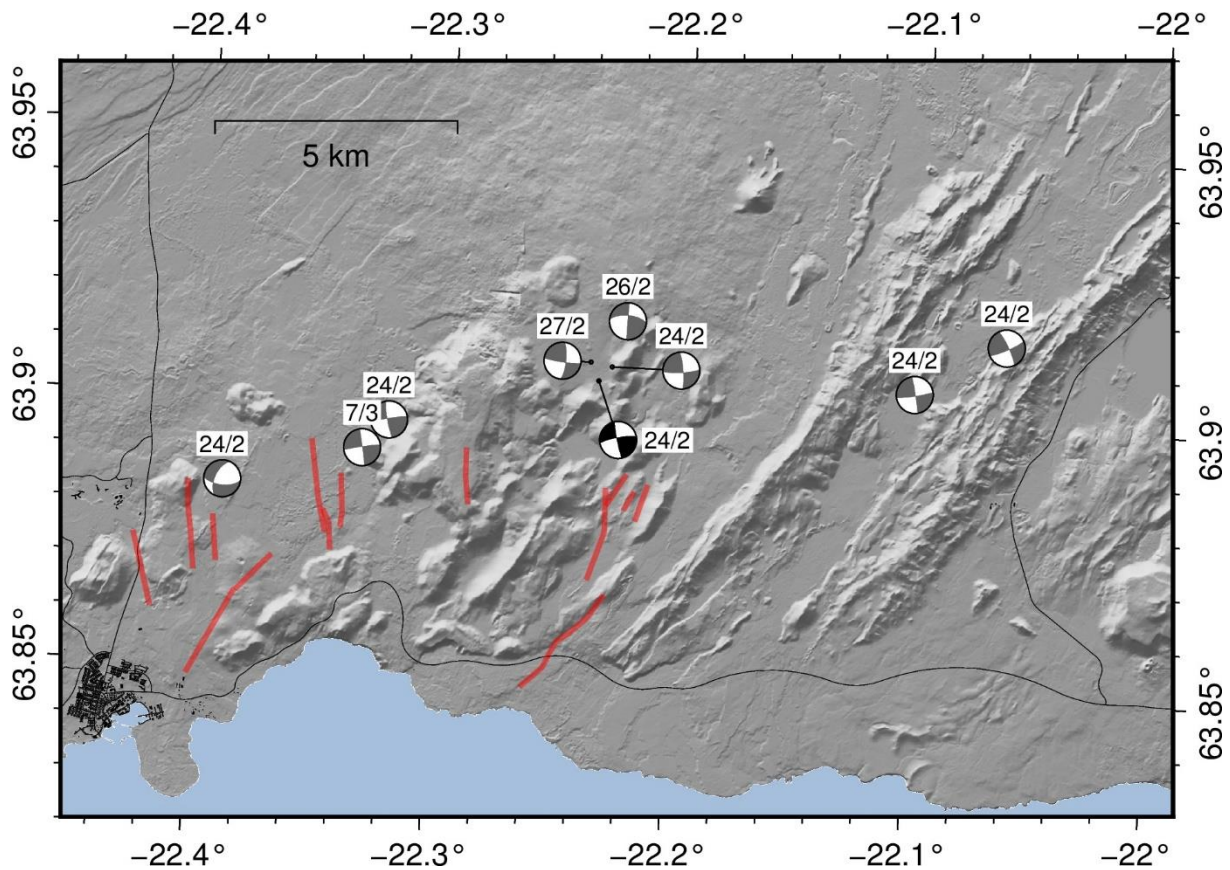


Figure 4. Focal mechanism of a selection of large earthquakes (magnitude > 4.8) that occurred on the 24th of February and onwards, shown in the location of the earthquake (data: Veðurstofa Íslands, Czech Academy of Science, ÍSOR, Orka náttúrunnar; processing: Þorbjörg Ágústsdóttir & Egill Árni Guðnason, ÍSOR). The date of the earthquake is indicated over the focal mechanism. The black focal mechanism is for the M5.7 earthquake. Background shows shaded topography, moving faults as inferred from InSAR (red lines), roads (black lines), buildings (black areas, and water (blue/grey areas).

3 Conclusions

As shown in this report, InSAR can be used to measure deformation over most of the Reykjanes Peninsula. This can be applied to long-term deformation spanning many years due to plate spreading and geothermal utilization, or much more brutal and short-term changes associated with large earthquakes or volcanic unrest. The large spatial coverage of InSAR allows to map the full extent of such deformation. The continuous deformation field provided by this technique can be used to derive areas of high strain, which are the most critical information for infrastructures.

4 References

- Björnsson S., Einarsson, P., Tulinius, H., and Hjartardóttir, Á. R. (2020). Seismicity of the Reykjanes Peninsula 1971–1976. *Journal of Volcanology and Geothermal Research*, 391, <https://doi.org/10.1016/j.jvolgeores.2018.04.026>.
- Drouin, V., Sigmundsson, F., Verhagen, S., Ófeigsson, B. G., Spaans, K., and Hreinsdóttir, S. (2017). Deformation at Krafla and Bjarnarflag geothermal areas, Northern Volcanic Zone of Iceland. 1993–2015, *Journal of Volcanology and Geothermal Research*, 344, 92–105, <https://doi.org/10.1016/j.jvolgeores.2017.06.013>.
- Drouin, V., and Sigmundsson, F. (2019). Countrywide observations of plate spreading and glacial isostatic adjustment in Iceland inferred by Sentinel-1 radar interferometry, 2015–2018. *Geophysical Research Letters*, 46, 8046–8055. <https://doi.org/10.1029/2019GL082629>
- Ferretti, A. et al. (2007). Submillimeter Accuracy of InSAR Time Series: Experimental Validation. *IEEE Transactions on Geoscience and Remote Sensing*, vol. 45, no. 5, 1142–1153, <https://doi.org/10.1109/TGRS.2007.894440>
- Juncu, D., Árnadóttir, T., Hooper, A., and Gunnarsson, G. (2017), Anthropogenic and natural ground deformation in the Hengill geothermal area, Iceland. *Journal of Geophysical Research: Solid Earth*, 122, 692–709, <https://doi.org/10.1002/2016JB013626>.
- Massonnet, D., Rossi, M., Carmona, C. et al. (1993) The displacement field of the Landers earthquake mapped by radar interferometry. *Nature* 364, 138–142. <https://doi.org/10.1038/364138a0>
- Pagli, C., Pedersen, R., Sigmundsson, F., and Feigl, K. L. (2003), Triggered fault slip on June 17, 2000 on the Reykjanes Peninsula, SW-Iceland captured by radar interferometry. *Geophysical Research Letters*, 30, 1273, <https://doi.org/10.1029/2002GL015310.6>
- Receveur, M., Sigmundsson, F., Drouin, V., and Parks, M. (2019). Ground deformation due to steam cap processes at Reykjanes, SW-Iceland: effects of geothermal exploitation inferred from interferometric analysis of Sentinel-1 images 2015–2017. *Geophysical Journal International*, 216 (3), 2183–2212, <https://doi.org/10.1093/gji/ggy540>
- Ruch, J., Wang, T., Xu, W. et al. (2016). Oblique rift opening revealed by reoccurring magma injection in central Iceland. *Nature Communication*, 7, 12352, <https://doi.org/10.1038/ncomms12352>
- Schlögel, R., Doubre, C., Malet, J.-P., and Masson, F. (2015) *Landslide deformation monitoring with ALOS/PALSAR imagery: A D-InSAR geomorphological interpretation method*, *Geomorphology*, 231, 314–330, <https://doi.org/10.1016/j.geomorph.2014.11.031>.
- Sigmundsson, F., Hreinsdóttir, S., Hooper, A. et al. (2010). Intrusion triggering of the 2010 Eyjafjallajökull explosive eruption. *Nature* 468, 426–430, <https://doi.org/10.1038/nature09558>
- Vadon, H., and Sigmundsson, F. (1997). Crustal Deformation from 1992 to 1995 at the Mid-Atlantic Ridge, Southwest Iceland, Mapped by Satellite Radar Interferometry. *Science*, 275 (5297), 193–197.
- Wang, T., Perissin, D., Rocca, F., and Liao, M.-S. (2011) Three Gorges Dam stability monitoring with time-series InSAR image analysis. *Science China Earth Sciences*, 54, 720–732, <https://doi.org/10.1007/s11430-010-4101-1>